Effect of gold(I) in the Room Temperature Phosphorescence of ethynylphenanthrene

Araceli de Aquino,[a,&] Francisco J. Caparrós,[a,b,&] Gabriel Aullón,[a,c] Jas S. Ward,[d] Kari Rissanen,[d] Yongsik Jung,[e] Hyeonho Choi,[e] João Carlos Lima,[f] Laura Rodríguez[a,b,*]

[a] *Departament de Química Inorgànica i Orgànica. Secció de Química Inorgànica. Universitat de Barcelona, Martí i Franquès 1-11, 08028 Barcelona, Spain. E-mail: laura.rodriguez@qi.ub.es*

[b] *Institut de Nanociència i Nanotecnologia (IN^{2}UB). Universitat de Barcelona, 08028 Barcelona (Spain)*

[c] *Institut de Química Teòrica i Computacional (IQTCUB). Universitat de Barcelona, 08028 Barcelona, Spain*

[d] *Department of Chemistry, University of Jyväskylä, P.O. Box 35, 40014, Jyväskylä, Finland.*

[e] *Samsung Advanced Institute of Technology, Samsung Electronics Co. Ltd., 130 Samsung-ro, Yeongtong-gu, Suwon-si, Gyeonggi-do, 16678, Republic of Korea*

[f] *LAQV-REQUIMTE, Departamento de Química, Universidade Nova de Lisboa, Monte de Caparica*

[&] Both authors contributed equally to this work

Abstract

The synthesis of two series of gold(I) complexes containing the general formulae PR_3-Au-C≡C-phenanthrene (PR_3 = PPh_3 (**1a**/**2a**), PMe_3 (**1b**/**2b**), $PNaph_3$ (**1c**/**2c**)) or (diphos)(Au-C≡C-phenanthrene)$_2$ (diphos = 1,1-*bis*(diphenylphosphino)methane, dppm (**1d**/**2d**); 1,4-*bis*(diphenylphosphino)butane, dppb (**1e**/**2e**)) have been synthesized. The two series differ on the position of the alkynyl substituent on the phenanthrene chromophore, being at the 9-position (9-ethynylphenanthrene) for the **L1**-series and at the 2-position (2-ethynylphenanthrene) for the **L2**-series. The compounds have been fully characterized by ^{1}H and ^{31}P NMR and IR spectroscopy, mass spectrometry and single crystal X-ray diffraction resolution in the case of compounds **1a**, **1e**, **2a**, and **2c**.

The emissive properties of the uncoordinated ligands and corresponding complexes have been studied in solution and within organic matrixes of different polarity (PMMA and Zeonex). We have observed room temperature phosphorescence (RTP) for all gold(I) complexes while only fluorescence can be detected for the pure organic chromophore. In particular, the **L2**-series present better luminescent properties regarding intensity of emission, quantum yields and RTP effect. Additionally, while the inclusion of all the compounds in organic matrixes induces an enhancement of the observed RTP due to the decrease in non-radiative deactivation, only the **L2**-series completely supress fluorescence giving rise to pure phosphorescent materials.

Keywords: Room temperature phosphorescence (RTP), gold, phenanthrene, Heavy atom effect, organic matrixes.

Introduction

Room-temperature phosphorescence (RTP) has become important for a variety of applications in different fields such as photodynamic therapy,[1] bioimaging,[2] optical limiting,[3] photon upconversion,[4] oxygen sensing,[5] and light-emitting diodes (OLEDs).[6] This phenomenon is difficult to be successfully achieved through pure organic molecules under normal conditions (room temperature and normal pressure) because of the weak spin-orbital coupling (SOC) between excited singlet and triplet states as well as the fast non-radiative deactivation of triplet excitons. Heavy-atom induced phosphorescence of organic chromophores that originates from SOC is a studied mechanism for RTP emitting materials due to the well-known heavy atom effect.[7–13] For these reasons, the phenomenon of RTP has become more popular for inorganic and organometallic complexes, easily containing heavy metal atoms, that exhibit strong RTP, mostly originating from the ^{3}MLCT transition.[14] The more favoured SOC process in the presence of heavy atoms is relevant for triplet state harvesting as a well-known procedure to achieve high intensities in light emitting devices, LEDs.[15] It must be considered that enhancing SOC by heavy atom effects affords an increase not only in the efficiency of triplet formation, ϕ_{ST}, and the radiative rate constant of the triplet, k_r^T, but also in the non-radiative rate constant for triplet deactivation k_{nr}^T. Nevertheless, the important point is that the increase in k_r^T and ϕ_{ST} must surpass the increase of k_{nr}^T to achieve a net gain in the emission RTP from the chromophores (Scheme 1).

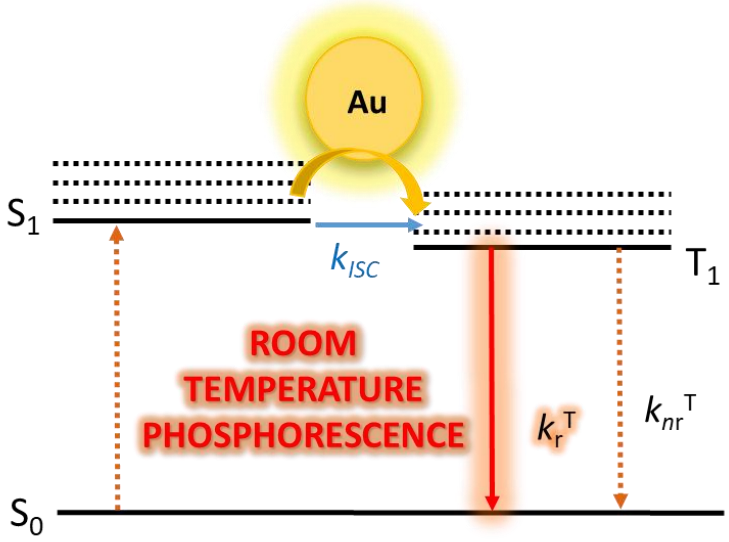

Scheme 1. Schematic representation of the photophysical pathways involved in these systems.

The chemistry of organogold(I) compounds is receiving much attention among heavy metal atom complexes. In comparison with the surrounding metals of the periodic table, gold displays a maximum relativistic effect which affects the resulting photophysical properties.[16–19] The formation of a gold(I)-carbon σ bond can significantly modify the electronic states of an organic chromophore by enhancing spin-orbit interactions, thus increasing the rate of intersystem crossing between singlet and triplet states with respect to the free aromatic counterpart.[20,21] In this way, while only fluorescence emission can be detected for specific organic luminophores, their corresponding organogold(I) compounds can exhibit dual luminescence (fluorescence and phosphorescence) at room temperature with emission yields that depend sensitively on the position of metal coordination.[17]

RTP is observed to be weakly recorded in solution. For this reason, some feasible strategies have been analysed for enhancing this RTP, such as crystal engineering,[22] polymerization,[23] aggregation,[24] or immobilization within organic matrixes[5]. All these mechanisms are focused to supress the non-radiative decay k_{nr} and the quenching k_q rate constants. In particular, the fabrication of thin films or matrix supports containing luminophores are highly desirable outside from academia for practical applications such as smart devices and luminescent sensors. This is due to their easily tune shape, size, flexibility or rigidity and to the fact that the resulting materials are much easier and simpler to handle in comparison with solution or powdered forms[25].

In this work, we present the synthesis and structural characterization of two series of ethynyl phenanthrene gold(I) compounds (**L1**-series and **L2**-series) that differ on the position of coordination of the gold(I) atom on the chromophore, changing the location of the alkynyl moiety. Their luminescent properties and, in particular, the resulting RTP behaviour have been carefully studied both in solution and when the samples are immobilized within organic matrixes with different polarity. The nuclearity of the compounds, steric hindrance, alkynyl position and polarity of the organic matrix have been evaluated as key parameters for obtaining RTP materials with increasing phosphorescence quantum yields and very long lifetimes in the order of hundreds of microseconds.

Results and Discussion.

Synthesis and characterization

A series of mono- and dinuclear gold(I) compounds containing, on one side, ethynylphenanthrene as chromophore and mono- or diphosphanes at the second coordination position have been synthesized following the reaction pathway shown below. The compounds have been obtained with two different isomers of ethynylphenanthrene, with the alkynyl group at 2- and 9- position. The 9-ethynylphenanthrene (**L1**) was commercially available while the 2-ethynylphenanthrene compound (**L2**) was synthesized by a Sonogashira coupling reaction from 2-bromophenanthrene and trimethylsilylacetylene in order to get the TMS-protected compound, **L2'**, and subsequent deprotection with K_2CO_3 to get the desired product, **L2**, in good yields (Scheme S1 and Figures S1-S2).

The reaction of **L1** or **L2** and AuCl(tht) in the presence of sodium acetate as a base gave rise to the formation of the insoluble polymers [Au-C≡C-phenanthrene]$_n$ (**1** and **2** respectively, from **L1** and **L2**) based on the procedure reported for similar gold polymers. The formation of the polymer has been evidenced by the disappearance of the C≡*C*-*H* vibration of the ethynylphenanthrene and the shift to shorter wavenumbers of the C≡C vibration in the corresponding IR spectra.

The reaction of a dichloromethane suspension of the polymer with the stoichiometric amount of mono- or diphosphanes allows the formation of the desired products (for PPh_3 (**1a**/**2a**), PMe_3 (**1b**/**2b**), $PNaph_3$ (**1c**/**2c**), dppm (**1d**/**2d**) and dppb (**1e**/**2e**), Scheme 2).

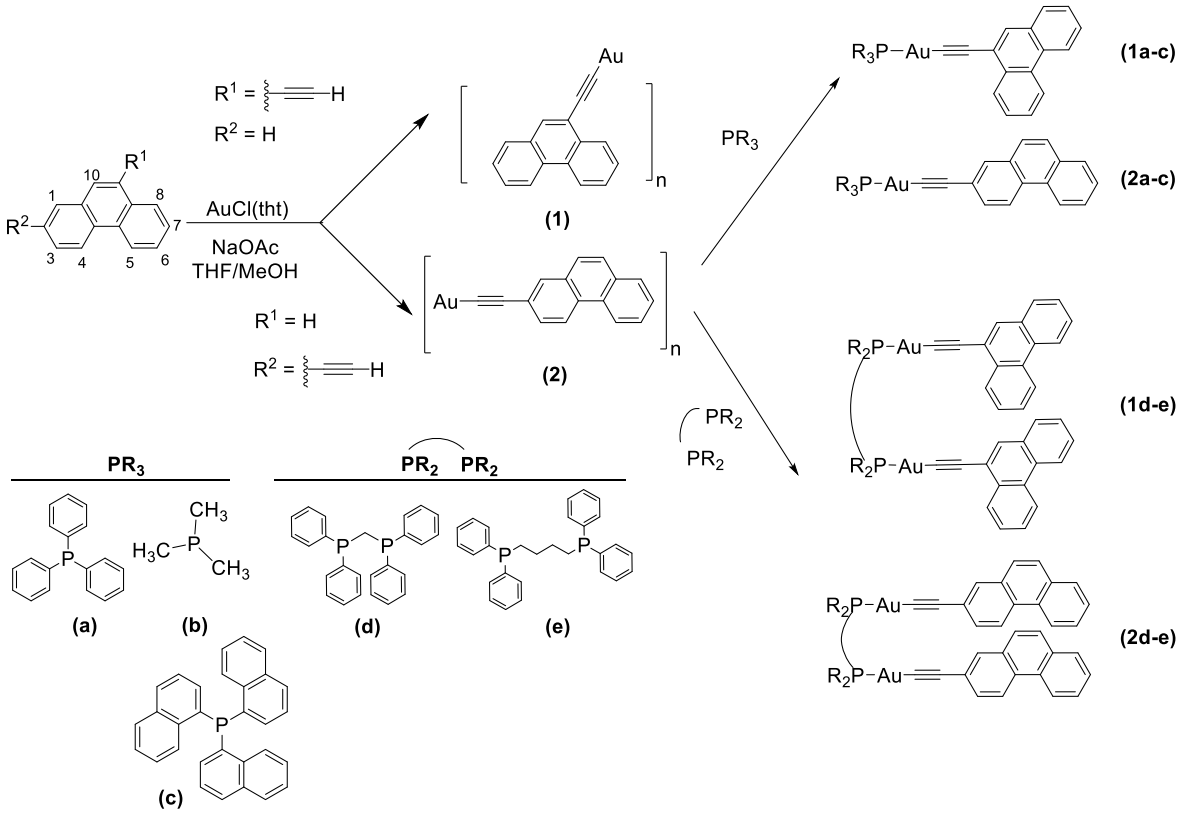

Scheme 2. Synthesis of the gold(I) complexes from the two different ethynylphenanthrene ligands **L1** and **L2**.

All gold complexes were successfully characterized by ^{1}H and ^{31}P NMR, IR and mass spectrometry. The ^{1}H NMR spectra show the signals of both the chromophore and the phosphane moieties with the expected integrations. Hydrogen atoms at positions 1, 2 and 4 (see position numbering in Scheme 2) are more affected by the coordination of the metal atom with a 0.1 ppm downfield shift. The $^{31}P\{^{1}H\}$ NMR spectra show in all cases one signal, as a direct indication of the formation of only one product, that is *ca*. 50-60 ppm downfield shifted with respect to the free phosphane, as previously observed in other similar reactions (Figures S3-S22).[24,26–31]

Mass spectrometry provided additional evidence for the successful formation of the complexes with the detection of the $[M + H^{+}]^{+}$ or $[M + Na^{+}]^{+}$ peak in all cases (see SI).

Single-crystals suitable for single X-ray diffraction were successfully obtained for **1a**, **1e**, **2a** and **2c** through slow diffusion of dichloromethane/hexane solutions of the compounds at room temperature. The corresponding molecular structures are presented in Figure 1 and the selected bond distances and angles are summarized in Table 1.

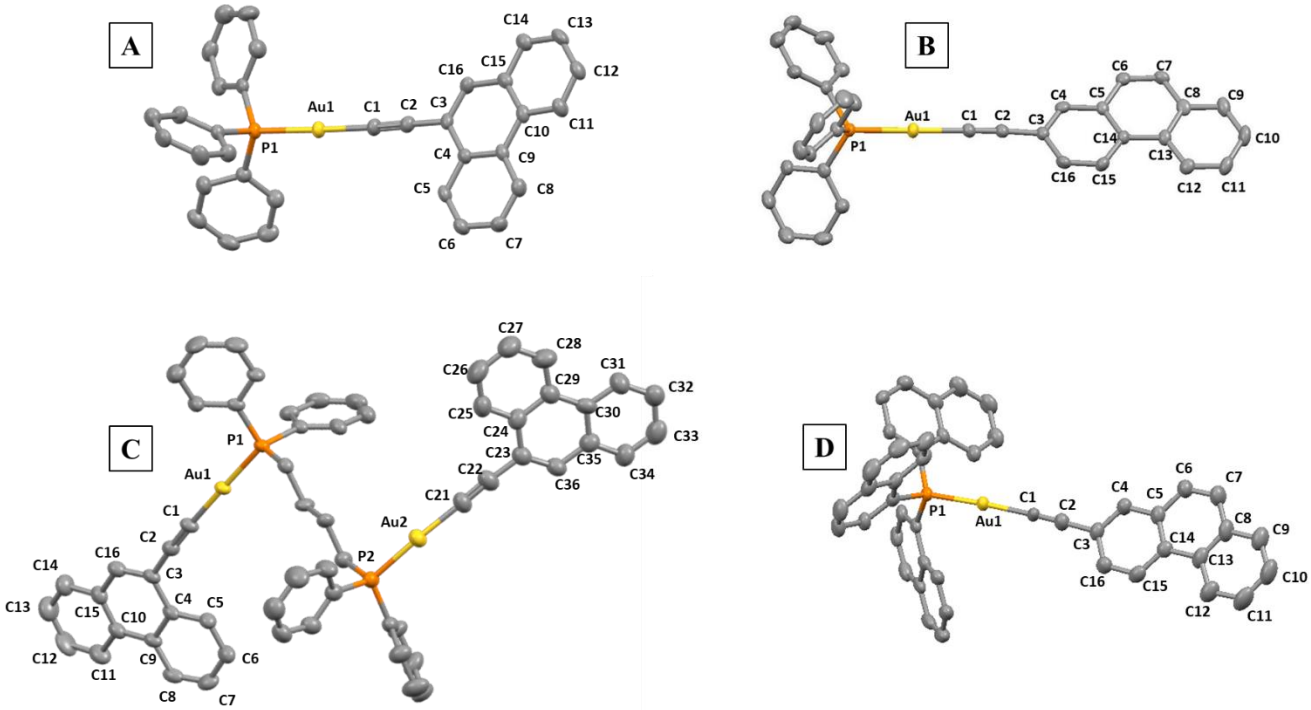

Figure 1. X-ray crystal structure of **1a** (A), **2a** (B), **1e** (C) and **2c** (D) (thermal ellipsoids at 50% probability; solvates and hydrogen atoms omitted for clarity). Yellow: gold; orange: phosphorus; grey: carbon. Hydrogens are omitted for clarity.

Table 1. Selected bond lengths (Å) and angles (º) for **1a**, **1e**, **2a** and **2c**.

Distance	**(Å)**	**Angle**	**(º)**
1a			
Au1-C1	2.001(7)	P1-Au1-C1	178.3(2)
Au1-P1	2.276(2)	Au1-C1-C2	177.7(6)
C1-C2	1.19(1)	C1-C2-C3	176.9(7)
C2-C3	1.448(9)		
2a			
Au1-C1	2.010(6)	P1-Au1-C1	179.0(2)
Au1-P1	2.277(1)	Au1-C1-C2	178.6(5)
C1-C2	1.181(7)	C1-C2-C3	175.0(6)
C2-C3	1.446(7)		
1e			
Au1-C1	1.993(6)	P1-Au1-C1	179.1(2)
Au1-C21	2.017(8)	P2-Au2-C21	172.6(7)
Au1-P1	2.276(1)	Au1-C1-C2	176.1
Au2-P2	2.267(2)	Au2-C21-C22	173.6(7)
C1-C2	1.203(8)	C1-C2-C3	175.1(7)
C21-C22	1.18(1)	C21-C22-C23	176.0(9)
C2-C3	1.451(8)		
C22-C23	1.45(1)		
2c			
Au1-C1	2.055(5)	P1-Au1-C1	177.0(1)
Au1-P1	2.282(1)	Au1-C1-C2	174.8(5)
C1-C2	1.137(7)	C1-C2-C3	176.1(7)
C2-C3	1.443(8)		

The Au-C and C≡C distances and P-Au-C and Au-C≡C angles (Table 1) are in the usual ranges for Au(I) alkynyl complexes.[28,31–41] Linear coordination of the phenanthrene ligands at the Au(I) centres is observed, with P-Au-C angles of 172.6-179.0º. The complexes display

a tetrahedral geometry at the hinge phosphorus atoms and near-linear geometry of the P-Au-C≡C- unit. No aurophilic contacts are observed in any of the structures.

The packing of **1a**, **1e** and **2a** complexes in the solid state displays a zig-zag conformation driven by the establishment of π···π (both between the phenanthrene and the π ring of the triphenylphosphane and between two phenanthrene rings), C-H···π interactions and Au···π[42] in the case of **1-2a** (Figures S33-S37). The two ethynylphenanthrene groups in **1e** are located in an antiparallel disposition and the resulting 3D packing displays the presence of inner cavities. The larger steric hindrance of the phosphane in **2c** induces an antiparallel disposition in the crystalline packing of the molecule (Figure S37).

H···Au interactions are also detected with distances of 3.290 (**1a**), 3.267 (**2a**), 2.943 (**1e**) and 3.133 (**2c**) Å respectively. These intermolecular interactions could be considered as hydrogen bonds that could have a very significant role in the packaging of these kind of molecules as it has been reported previously.[33,34,43–47]

It seems that the large aromaticity of the phenanthrene group favours these kind of intermolecular contacts with respect to possible aurophilic interactions, usual in gold(I) complexes. These contacts may be also hindered by the bulkiness of the phenyl groups unless the two Au(I) atoms may be located at the adequate distance such as in the case of dppm derivative (see below photophysical behaviour).

Photophysical characterization

The absorption and emission spectra of all the complexes **1a-e** and **2a-e** and of the free ligands **L1** and **L2** were recorded in $1x10^{-5}$ M acetonitrile solutions (except **1c**, which was recorded in THF due to its low solubility in acetonitrile) at room temperature and the obtained data are summarized in Table 2.

The electronic absorption spectra of all the compounds (Figure 2) show an intense band with vibronic resolution at 310-330 nm. These bands display the same profile as the corresponding spectrum of the **L1** and **L2** ligands, but are red-shifted due to coordination to the metal atom and thus they are assigned to metal perturbed π–π* intraligand

transitions.[14,48–50] Additionally, all the absorption bands are 10-20 nm blue-shifted for all **L2** and corresponding complexes compared with the analogous **L1**-compounds.

An additional absorption band centered at 300 nm appears for **1c**/**2c**, that contain the trinaphthylphosphane ($PNaph_3$) ligand, which is ascribed to the π-π*($Naph_3$) transition.[31] In the case of **1d**/**2d**, a lower-energy absorption band is observed as a tail which has been assigned to the absorption of aggregates and arises from σ*(Au···Au)-π* transitions, as an indication of the possible aurophilic contacts in solution for these complexes.[51]

Table 2. Absorption and emission data of **L1**, **L2** and the compounds **1a-e** and **2a-e** in acetonitrile at $1x10^{-5}$ M (λ_{exc}=328 nm for **L1** series and λ_{exc} = 315 nm for **L2** series) and ratio of phosphorescence and fluorescence intensities, I_P/I_F, without O_2. [a] Measurements in THF.

Compound	Absorption λ_{max} (nm) (ε 10^4 $M^{-1}\cdot cm^{-1}$)	Fluorescence Emission (solution, λ_{max} (nm)) air-equilibrated	Phosphorescence Emission (solution, λ_{max} (nm)) without O_2	I_P/I_F
L1	299 (1.68), 311 (2.05)	378	-	-
1a	311 (2.45), 328 (3.21)	387	533, 579	2.8
1b	311 (1.58), 328 (2.03)	387	533, 579	0.2
1c[a]	300 (2.34), 311 (2.51), 333 (2.30)	387	533, 579	0.15
1d	311 (4.06), 328 (3.99)	387	538, 579	2.3
1e	311 (5.25), 328 (6.69)	387	533, 579	0.05
L2	263 (6.7), 290 (2.21)	381	-	-
2a	278 (3.41), 315 (2.58)	384	508	12.4
2b	278 (3.12), 315 (1.87)	384	508	9.1
2c	279 (5.08), 317 (4.23), 330 (1.05)	373, 388	477, 511	1.7
2d	278 (9.55), 315 (5.07)	384	508	3.5
2e	278 (5.49), 315 (3.13)	384	508	7.7

The emission spectra of all the compounds were recorded in the presence and absence of O_2 (Figure 2 and S38-S39). A vibronically structured band centered at *ca*. 385 nm can be detected in all compounds in air-equilibrated samples with 5-10 nm red-shift upon coordination of the Au-PR_3 fragment. The emission of **L2**-compounds is around 3 nm blue-

shifted with respect to **L1**-compounds. The small Stokes' shift and the vibronical spacings of 1490 cm^{-1} (for **L1**-series) and 1377 cm^{-1} (for **L2** series), corresponding to the C=C vibrations, provides the corroboration to confidently assign them as ^{1}IL fluorescence transitions. A second weak emission band around 510 nm appears for all **L2**-complexes (not for the free ligand) and is only detected for **1a** and **1d**. This band becomes much more intense after removing oxygen to the solution (Figure 2 right). The large Stokes' shift together with the oxygen-sensitive intensity and the vibronically structured shape again provides sufficient corroboration to confidently assign it to the phosphorescence ^{3}IL transitions.[14,48,50]

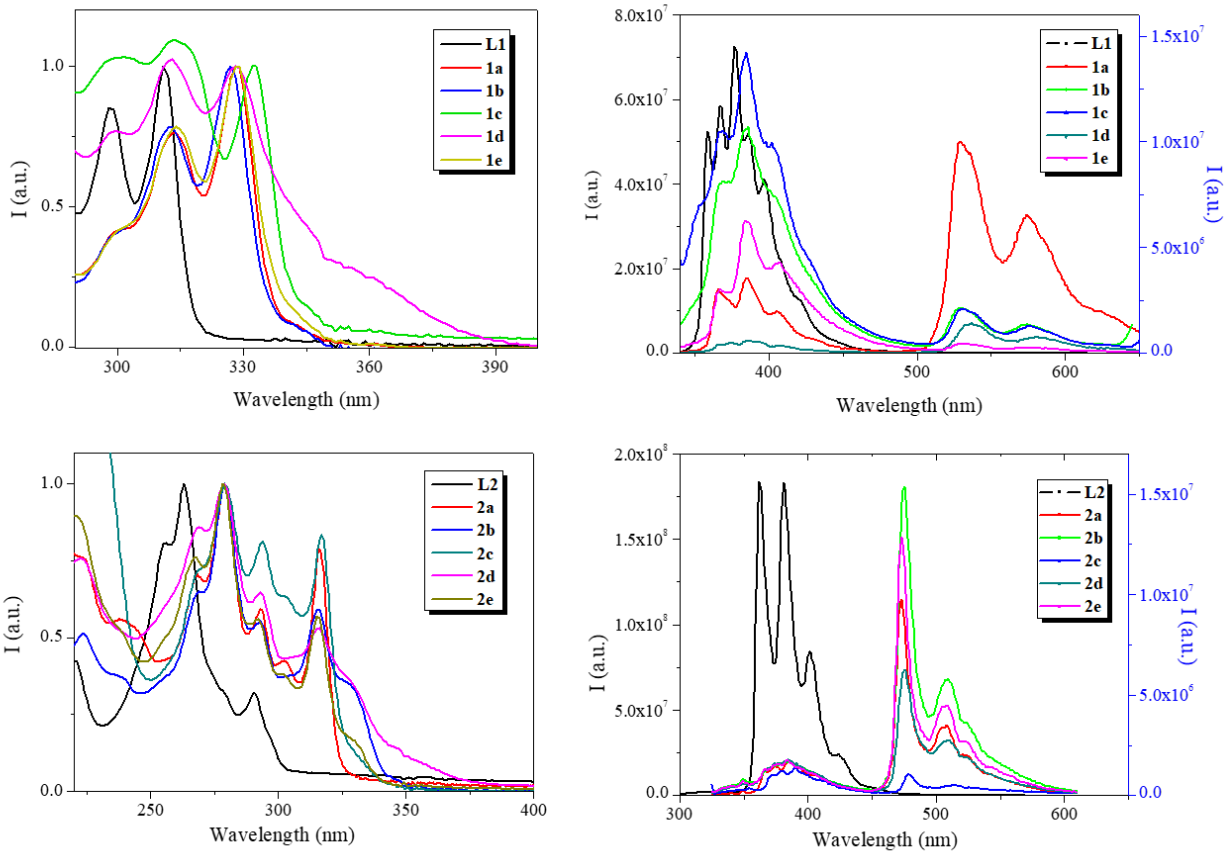

Figure 2. Absorption (left) and emission N_2-saturated samples (right) spectra of **L1** (above) and **L2** -derivatives (below) in $1 \cdot 10^{-5}$ M acetonitrile (except **1c**, which was in THF) solutions.

Interestingly, the change on the alkynyl position from 9-ethynylphenanthrene to 2-ethynylphenanthrene) is favoring phosphorescence emission in all cases. It can be observed that the phosphorescence emission is only especially relevant for deoxygenated samples of the PPh_3 and dppm derivatives in the **L1**-derivatives (compounds **1a** and **1d**, respectively), as the observed emissions for the rest of **L1**-series were dominated by the fluorescence. On the contrary, phosphorescence was much more favored in all the **L2**-derivatives, with the Phosphorescence/Fluorescence intensity ratio increased by 12-fold for the PPh_3 complex, **2a** (see Table 2). This is also evidenced in the corresponding phosphorescence quantum yields, ϕ_P, which are one order of magnitude larger than the corresponding fluorescence data, ϕ_F, in all the **L2**- gold(I) complexes except for **2e** (the dppb derivative) with a comparatively lower difference though still 5 times larger. Moderately large ϕ_P values (2-3-fold with respect to ϕ_F) were measured for the **L1**-compounds (see Table 3).

The generally large values of room temperature phosphorescence in the **L2**-derivatives might be related either to the lower steric hindrance of the resulting complexes derived from 2-ethynylphenanthrene with higher linearity in comparison to the 9-ethynylphenanthrene data where the chromophore was in a perpendicular disposition with the alkynyl edge, or other electronic aspects that deserve future investigation.

Phosphorescence emission cannot be detected for the free ligands **L1** and **L2**, providing direct evidence of the role of gold(I) heavy atom in the intersystem crossing and phosphorescence emission at room temperature.

Table 3. Luminescent quantum yields in N_2-saturated samples.

L1-series			L2-series		
Compound	**ΦFl**	**ΦPh**	**Compound**	**ΦFl**	**ΦPh**
L1	0.116	0	**L2**	0.209	0
1a	0.005	0.013	**2a**	0.209	0
1b	0.007	0.019	**2b**	0.001	0.035
1c	0.061	0.001	**2c**	0.003	0.033
1d	0.010	0.034	**2d**	0.005	0.053
1e	0.007	0.022	**2e**	0.005	0.035

In order to minimize the non-radiative processes and maximize the RTP, the samples were immobilized within two different organic matrixes, polymethylmetacrylate (PMMA) and Zeonex 480. As found previously in solution, RTP is more favoured for the **L2**-series where the almost complete disappearance of fluorescence in all gold complexes was observed, giving rise to effectively pure phosphorescent materials subsequent to removing oxygen (Figures 3 and 4). RTP is also favoured to some extend for the **L1**-series when the compounds are immobilized in these matrixes (Figure S40), in particular for the dppm derivative, **1d**. This may be due to the scalability of the intersystem crossing due to Au(I)···Au(I) intramolecular contacts.

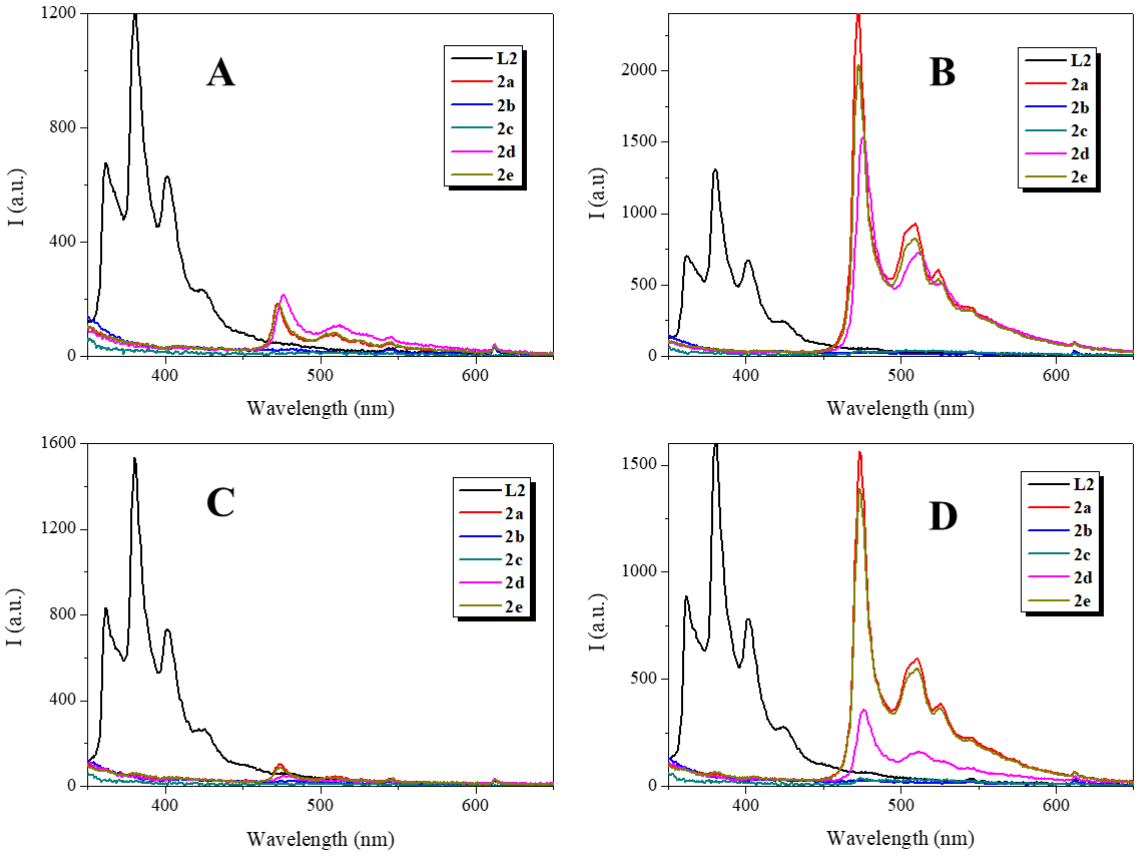

Figure 3. Emission spectra of the compounds **L2**, **2a-d** immobilized in PMMA with (**A**) and without (**B**) oxygen and Zeonex with (**C**) and without (**D**) oxygen (λ_{exc} = 285 nm).

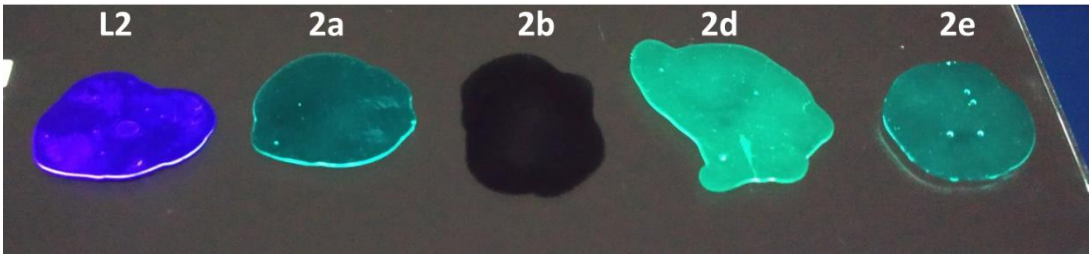

Figure 4. Image of **L2**-compounds immobilized in PMMA (λ_{exc} = 254 nm)

Luminescence quantum yields were also measured in all cases for the prepared doped-matrix samples (Table 4). In this way, the improvement of the RTP can be quantitatively measured for both series. Although an important increase of one order of magnitude can be

detected in the **L1**-series, important RTP quantum yield values in the order of 25-29 % were recorded for the **2a**, **2d** and **2e** gold complexes in PMMA and were in the order of 20% in Zeonex.

Phosphorescence emission cannot be detected for the **L1** and **L2** uncomplexed systems, as previously observed in solution, providing direct evidence of the role of the gold(I) heavy metal atom in the intersystem crossing and phosphorescence emission at room temperature.

Luminescence lifetimes in the order of hundreds of microseconds were measured for all the samples embedded within the PMMA and Zeonex matrixes (Table 5), strongly supporting the origin of the phosphorescence emission. Interestingly, very long lifetimes can be recorded, making these samples very appealing as luminescent materials. These values are much larger than the previously reported triplet lifetime of phenanthrene in PMMA (0.77 s).[52] Additionally, calculation of the corresponding radiative and non-radiative rate constants, from the ϕ and τ values, demonstrated that, as expected, the non-radiative relaxation is less favored in PMMA (Table 6). The largest k_r calculated value for **2d** (1877.7 s^{-1}) is *ca*. 4 orders of magnitude larger than that previously reported for phenanthrene (0.26 s^{-1}).[14]

Table 4. Fluorescence and Phosphorescence quantum yields of the **L1**- and **L2**-series of compounds included within PMMA and Zeonex (as N_2-saturated films). The best values are highlighted in grey. [a]**1c** could not be immobilized in these matrixes due to its low solubility in the corresponding media.

Compound	ΦFl		ΦPh	
	PMMA	**Zeonex**	**PMMA**	**Zeonex**
L1	0.082	0.090	0	0
1a	0.006	0.005	0.059	0.051
1b	0.006	0.005	0.072	0.059
1c[a]	-	-	-	-
1d	0.002	0.004	0.102	0.020
1e	0.005	0.004	0.073	0.039
L2	0.131	0.163	0	0
2a	-	-	0.290	0.186
2b	-	-	0.005	0.005
2c	-	-	0.022	0.022
2d	-	-	0.253	0.069
2e	-	-	0.280	0.175

Table 5. Luminescent lifetimes measured for deoxygenated samples included in PMMA and Zeonex matrixes. [a] Samples not possible to prepare due to the insolubility of the compound in the matrixes. [b] Almost non emissive material.

Compound	τ(μs)	
	PMMA	Zeonex
1a	231.84	145.00
1b	272.74	256.96
1c	- [a]	- [a]
1d	330.83	112.03
1e	186.57	232.24
2a	362.13	305.32
2b	- [b]	- [b]
2c	503.31	318.90
2d	132.61	296.12
2e	787.9	130.9

Table 6. Ratiative (k_r) and non-radiative (k_{nr}) rate constants calculated for all the compounds in both deoxygenated PMMA and Zeonex matrixes. The best values are highlighted in grey.

Compound	PMMA		Zeonex		k_{nr}/k_r	
	k_r (s^{-1})	k_{nr} (s^{-1})	k_r (s^{-1})	k_{nr} (s^{-1})	PMMA	Zeonex
1a	254.5	4058.8	351.7	6544.8	15.9	18.6
1b	264.0	3402.5	229.6	3662.0	12.9	15.9
1c	-	-	-	-	-	-
1d	308.3	2714.4	178.5	8747.7	8.8	49.0
1e	385.9	4974.0	167.9	4138.0	12.9	24.6
2a	787.0	1974.4	609.2	2666.1	2.5	4.4
2b	-	-	-	-	-	-
2c	43.7	1943.1	69.0	3066.8	44.5	44.5
2d	1877.7	5663.2	229.6	3147.4	3.0	13.7
2e	355.4	913.8	1298.7	6340.7	2.6	4.9

Theoretical calculations

TD-DFT calculations were carried out to determine the excited states and their involved molecular orbitals in acetonitrile solution (see Table S7 and Figure S41). For each series, the same compounds were studied containing the different phosphanes: PPh_3, PMe_3, $PNaph_3$, and $PMePh_2$ (this can provide results those will be compared with bimetallic species in the absence of metal···metal interactions).

For the **L1** series (9-ethynylphenanthrene), two bands are calculated at 3.5 and 4.2 eV corresponding to transitions between π orbitals of the phenanthrene rings (Table S8). The first band is always most intense and it is assigned to HOMO→LUMO transition ($f \approx 1.0$), being these orbitals centred in the phenanthrene rings (~70 %) with an important contribution of C≡C fragment. The second one is found for HOMO-1→LUMO transition ($f \approx 0.34$), being the HOMO-1 is only a phenanthrene orbital (> 95 %). Those related triplet states are located at 2.3 and 3.8 eV, respectively. Since that this description is found for PPh_3 (**1a**), PMe_3 (**1b**) and $PMePh_2$ derivatives, one can expect identically values of photochemical properties for dppb compound (**1e**) where metal···metal interaction is absence (optimized distance about 9 Å), and probably for dppm compound (**1d**, ~ 3.7 Å). However, more complex situation is found for $PNaph_3$ (**1c**) because several transitions are expected between these two bands involving the naphthyl groups of the phosphane.

For the **L2** series (2-ethynylphenanthrene), three bands are now calculated between 3.7 and 4.2 eV between two occupied and two empty π orbitals (with the triplet states between 2.6 and 3.4 eV, Table S9). The first band is newly most intense of three ($f \approx 1.4$, 0.9 and 0.3, respectively), and it corresponds to HOMO→LUMO transition as previously is shown for **L1** series. The second is found for HOMO-1→LUMO+1 transition, and it can classify as intraligand charge-transfer of the phenanthrene due the composition of these two orbitals (> 95 %). The third is much weaker and it results of the combination of two monoexcitations of those orbitals, HOMO→LUMO+1 and HOMO-1→LUMO. This description is applied to PPh_3 (**2a**), PMe_3 (**2b**) and $PMePh_2$ derivatives, latter can extrapolate to bridging diphosphanes (**1d** and **1e**). Additionally, $PNaph_3$ compound (**2c**) presents additional transitions by the naphthyl groups of the phosphane.

Finally, comparing the effect of the phosphane, similar photochemical properties are expected for PPh_3 and PMe_3. Moreover, $PNaph_3$ compounds present poor activity due the lower oscillator strength and the interference of other monoexcitations of the naphtyl groups. In the case of diphosphanes, the calculations show the presence of two independent chromophores for dppb derivatives in agreement to large Au···Au distance in the most favourable conformation (about 9 Å). Nevertheless, similar situation is found for dppm having a splitting of less than 4 nm (Au···Au distances are calculated at 4.4 and 3.7 Å for **1d**

and **2d**, respectively), but their conformation can easily modified and the presence Au···Au contacts would provide major changes.

Interestingly, we can observe that the triplet state closer in energy to the S1 appears slightly at higher energy in the **L1** series. On the contrary, the corresponding triplet state in **L2**-series is lower in energy to S1 (see Figure 5). This means that the population of the triplet state in **L2** complexes is much more favoured than in **L1** and for this, RTP process is more efficient.

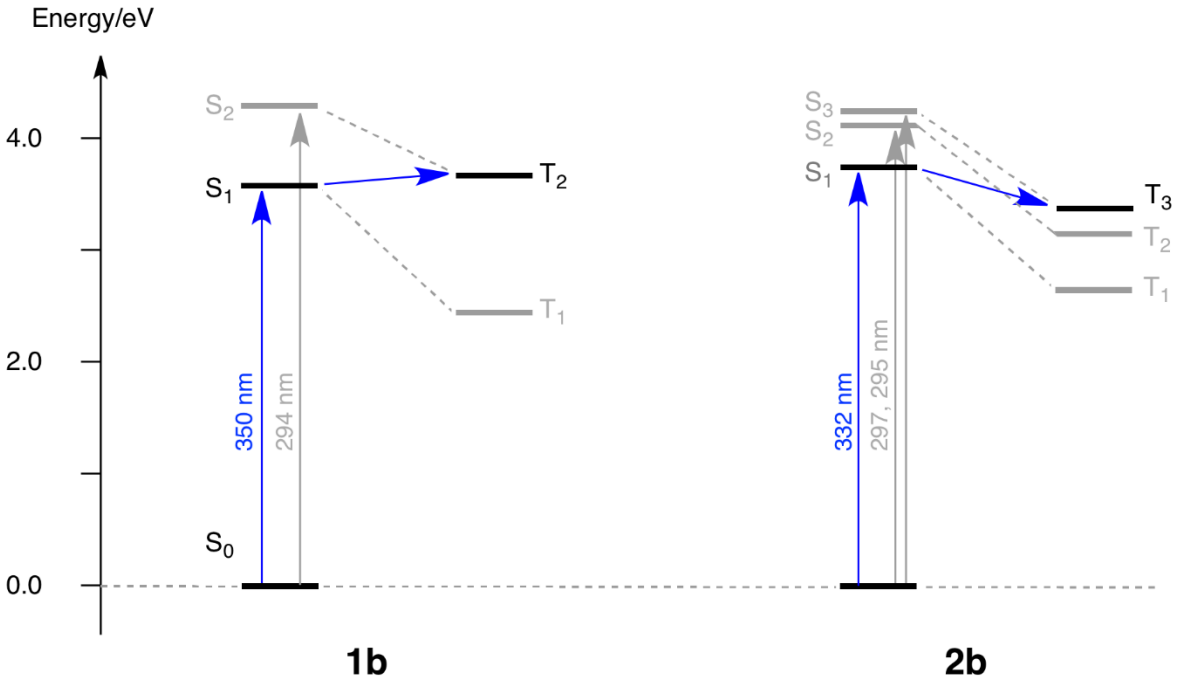

Figure 5. Schematic representation of the calculated lower singlet and triplet states of **1b** (left) and **2b** (right).

Conclusions

The position of the alkynyl moiety at the phenanthrene chromophore determines the resulting 3D structure of the synthesized gold(I) complexes and their luminescent properties. The synthesis of two series of gold(I)-alkynylphenanthrenes containing the chromophore in linear (**L2**-series) or perpendicular disposition (**L1**-series) demonstrates that linear disposition of the chromophores induces a clear enhancement of the RTP phenomenon. This RTP is observed in all gold(I) complexes due to the heavy atom effect while no phosphorescence can be recorded for free organic molecules.

The presence of an organic environment such as the PMMA matrix has been observed to be a very good way to improve RTP.

Luminescent lifetimes in the order of hundreds of microseconds are perfectly in agreement with the phosphorescence emission and indicate the successful synthesis of very promising phosphorescent materials. Calculation of radiative and non-radiative rate constants indicate that the main reason for the lower phosphorescence recorded in Zeonex compared with that recorded in PMMA may be due to more favored deactivation processes in this matrix.

TD-DFT theoretical calculations let us to identify the energies of the lowest energy singlet excited state, S1 and the corresponding closer triplet state. The population of the triplet state is expected to be much more favored in **L2**-series in agreement with the more favored non-radiative deactivation process and the lower RTP effect.

Experimental section

General procedures

All manipulations have been performed under prepurified N_2 using standard Schlenk techniques. All solvents have been distilled from appropriated drying agents. Commercial reagents PPh_3, PMe_3, $P(1\text{-Naph})_3$, dppm, dppb and PMMA were purchased from Aldrich, and 2-bromophenanthrene was purchased from Fluorochem.

Crystal data

The crystal data and experimental details for the data collection are given in Tables S1-S4. The single crystal data for **1a**, **1e** and **2a** were measured using a Bruker-Nonius KappaCCD diffractometer with an APEX-II detector with graphite-monochromatized Mo-*K*α (λ = 0.71073 Å) radiation. Data collection and reduction were performed using the program *COLLECT*[53] and *HKL DENZO AND SCALEPACK*[54] respectively, and the intensities were corrected for absorption using *SADABS*.[55] The single crystal data for **2c** was collected using a Rigaku-Oxford Diffraction SuperNova dual-source diffractometer with an Atlas CCD detector using mirror-monochromated Cu-Kα (λ = 1.54184 Å) radiation. The data collection and reduction were performed using the program CrysAlisPro and Gaussian face index absorption correction method was applied. The structures were all solved by intrinsic phasing (*SHELXT*)[56] and refined by full-matrix least squares on F^2 using the *OLEX2* software,[57] which utilizes the *SHELXL-2014* module.[58] CCDC-2019549 to CCDC-2019552 contain the supplementary crystallographic data for these structures. These data can be obtained free of charge from The Cambridge Crystallographic Data Centre via www.ccdc.cam.ac.uk/data_request/cif.

Physical measurements

Infrared spectra have been recorded on a FT-IR 520 Nicolet Spectrophotometer. ^{1}H NMR (δ(TMS) = 0.0 ppm) and $^{31}P\{^1H\}$ NMR (δ(85% H_3PO_4) = 0.0 ppm) spectra have been obtained on a Varian Mercury 400 and Bruker 400. ES(+) mass spectra were recorded on a Fisons VG Quatro spectrometer. Absorption spectra have been recorded on a Varian Cary 100 Bio UV-Spectrophotometer and emission spectra on a Horiba-Jobin-Ybon SPEX Nanolog Spectrofluorimeter.

Theoretical Calculations.

Density functional calculations were carried out using the GAUSSIAN package.[59] The hybrid density function method known as B3LYP was applied.[60,61] Effective core potentials (ECP) were used to represent the innermost electrons of the gold atom and the basis set of valence triple-ζ quality with an extra d-polarization function.[62] A similar description was used for all main group elements. [63] Atomic charges and populations analysis have been confirmed from analysis of Natural Bond Order. [64] Solvent effects of acetonitrile were taken into account by PCM calculations, [65] keeping the optimized geometries for the gas phase without symmetry restrictions. Excited states and absorption spectra were obtained from the time-depending algorithm implemented in Gaussian09. [66]

Synthesis and characterization

Hydrogen atoms assignment is described in Scheme 1.

Synthesis of **L2'**.

2-bromophenanthrene (400 mg, 1.56 mmol) was added to a mixture of THF and diisopropylamine (v/v = 1.5:1). Then, CuI (1.52 mg, 0.008 mmol), $PdCl_2(PPh_3)_2$ (14.0 mg, 0.02 mmol) and ethynylmethylsilane (153.11 mg, 1.56 mmol) were added to the solution and the reaction mixture was maintained under stirring for 2 days at 50ºC. After this time, the solution was cooled to room temperature and concentrated to dryness under reduced pressure. The product was obtained after purification through column chromatography by using dichloromethane and hexane (v/v = 1:1). Yield: 98 mg, ɳ = 92 %. ^{1}H NMR (400 MHz, CD_3Cl) δ 8.64 (dd, J = 8.2, 1.4 Hz, $1H_4$), 8.60 (dd, J = 8.5, 0.7 Hz, $1H_5$), 8.03 (d, J = 1.8 Hz, $1H_1$), 7.88 (dd, J = 7.6, 1.5 Hz, $1H_3$), 7.76 – 7.58 (m, $5H_{6\text{-}10}$), 0.30 (s, $9H_{SiMe3}$). IR ($\bar{\upsilon}$, cm^{-1}): ν(C≡C) at 2108 cm^{-1}.

Synthesis of **L2**

K_2CO_3 (862.4 mg, 6.24 mmols) was added to a solution of **L2'** (427.6 mg, 1.56 mmols) in 10 ml of a solution of dichloromethane/methanol (v/v = 1:1). The mixture was stirred for 5 h at room temperature. Then, the solvent was evaporated, and the compound was extracted

with dichlormethane/water. The organic phase was dried with $MgSO_4$ and concentrated to dryness. Yield: 295.7 mg, η = 94%. ^{1}H NMR (400 MHz, CD_3Cl) δ 8.64 (td, J = 8.7, 1.7 Hz, $2H_{4,5}$), 8.06 (d, J = 1.8 Hz, $1H_1$), 7.89 (dd, J = 7.7, 1.6 Hz, $1H_3$), 7.79 – 7.59 (m, $5H_{6\text{-}10}$), 3.19 (s, $1H_{terminal}$). MALDI-TOF MS (+) m/z: 427.1455 ($[2M + Na]^+$, calc.: 427.1463), 256.2321 $[M + Na + MeOH]^+$, (calc. 257.2391). IR ($\bar{\upsilon}$, cm^{-1}): ν(C≡*C*-*H*) at 3284 cm^{-1}; ν(C≡C) at 2100 cm^{-1}.

Synthesis of **1**.

For the formation of the gold polymer (**1**), a solution of **L1** (100 mg, 0.5 mmol) in 10 ml of THF/MeOH (v/v = 1:1) was added to a mixture of AuCl(tht) (156.4 mg, 0.5 mmol) and CH_3COONa (200.8 mg, 1 mmol), instantly generating an orange precipitate. The solution was stirred for 1 h. The solid was isolated by filtration yielding 149 mg (η=75%). IR ($\bar{\upsilon}$, cm^{-1}): ν(C≡C) 2027.

Synthesis of **2**.

A solution of **L2** (80 mg, 0.396 mmol) in 10 ml of THF/MeOH (v/v = 1:1) was prepared and then, AuCl(tht) (126.95 mg, 0.396 mmol) and CH_3COONa (65.01 mg, 0.792 mmol) were added to the reaction mixture. An orange precipitate was formed, and the solution was stirred for 1 h at room temperature. The solid was isolated by filtration yielding 110 mg (η = 70%). IR ($\bar{\upsilon}$, cm^{-1}): ν(C≡C) 1994.

Synthesis of **1a**.

A solution of PPh_3 (13 mg, 0.05 mmol) in 15 ml of CH_2Cl_2 was added to **1** (20 mg, 0.05 mmol), and the mixture stirred for 1 h. The solution was reduced to half of the volume and the product was precipitated by the addition of hexane. The product was recrystallized with CH_2Cl_2/hexane yielding 16 mg of **1a** (η=48%). ^{1}H-NMR (400 MHz, $CDCl_3$): δ 8.75-8.80 (m, 1H, H_5), 8.60-8.69 (m, 2H, $H_{4,8}$), 8.05 (s, 1H, H_{10}), 7.81 (d, J=7.7, 1H, H_1), 7.44-7.68 (m, 19H, $H_{2,3,6,7,\ Ph}$). ^{31}P{1H} NMR (161.9 MHz, $CDCl_3$, ppm): δ 42.2 (s). HR ESI-MS (+) m/z: 683.111 ($[M + Na]^+$, calc. 683.120). IR ($\bar{\upsilon}$, cm^{-1}): ν(C≡C) 2109 cm^{-1}; ν(C=C) 1434; 1488; ν(P-C) 1100.

Synthesis of **1b**.

Complex **1b** was synthesized following similar procedure detailed for **1a** but using PMe_3 (4 mg, 0.05 mmol) instead of PPh_3. Yield: 10 mg (ɳ=42%). ^{1}H-NMR (400 MHz, $CDCl_3$): ^{1}H-NMR (400 MHz, $CDCl_3$): δ 8.72 (d, J = 7.3 Hz, 1H, H_5), 8.58-8.68 (m, 2H, $H_{4,8}$), 8.01 (s, 1H, H_{10}), 7.79 (d, J = 7.8 Hz, 1H, H_1), 7.68 – 7.50 (m, 4H, $H_{2,3,6,7}$), 1.58 (d, J=10.1Hz , 9H, H_{Me}). ^{31}P{1H} NMR (161.9 MHz, $CDCl_3$, ppm): δ 0.87 (s). HR ESI-MS (+) m/z: 497.069 ($[M+Na]^+$, calc: 497.071). IR ($\bar{\upsilon}$, cm^{-1}): ν(C≡C) at 2072 cm^{-1}; ν(C=C) 1478, 1435; ν(P-C)1100.

Synthesis of **1c**.

Complex **1c** was synthesized following similar procedure detailed for **1a** but using $P(Naph)_3$ (20.6 mg, 0.05 mmol) instead of PPh_3. Yield: 16.6 mg (ɳ=41%). ^{1}H-NMR (400 MHz, DMSO): δ 8.79 (d, J=7.9 Hz, 1H, H_8), 8.74 (d, J=7.6 Hz, 2H, $H_{4,5}$), 8.42 (d, J=7.6 Hz, 1H, H_8), 8.31 (d, J=8.6 Hz, 2H, $H_{3,6}$), 8.17-8.23 (m, 2H, $H_{2,7}$), 7.85 (s, 1H, H_{10}), 7.20-7.76 (m, 21H, H_{PNaph3}). ^{31}P{^{1}H} NMR (161.9 MHz DMSO, ppm): δ -34.6 (s). HR ESI-MS (+) m/z: 811.190 ($[M+H^+]$, calc. 811.183). IR ($\bar{\upsilon}$, cm^{-1}): ν(C≡C) 2122 cm^{-1}; ν(C=C) 1490, 1450; ν(P-C) 1066.

Synthesis of **1d**.

Complex **1d** was synthesized following similar procedure detailed for **1a** but using dppm (9.6 mg, 0.025 mmol) instead of PPh_3. Yield: 14 mg (ɳ=48%). ^{1}H-NMR (400 MHz, $CDCl_3$): δ 8.63-8.73 (m, 4H, $H_{4,5}$), 8.37-8.41 (m, 2H, H_1), 8.02 (s, 2H, H_{10}), 7.85 (d, J=7.9 Hz, 2H, H_8), 7.57-7.76 (m, 20H, H_{Ph}), 7.39-7.55 (m, 8H, $H_{2,3,6,7}$), 3.60 (t, J=11.2 Hz, 2H, H_{CH2}), ^{31}P{1H} NMR (161.9 MHz $CDCl_3$, ppm): δ 23.8 (s). MALDI-TOF MS (+) m/z: 1181.284 ($[M+H^+]$, calc.: 1181.200). IR ($\bar{\upsilon}$, cm^{-1}): ν(C≡C) 2084 cm^{-1}; ν(C=C) 1482; 1434; ν(P-C) 1099.

Synthesis of **1e**.

Complex **1e** was synthesized following similar procedure detailed for **1a** but using dppb (10.7 mg, 0.025 mmol) instead of PPh_3. Yield: 16.2 mg (ɳ=53%).^{1}H-NMR (400 MHz, $CDCl_3$): 8.74-8.79 (m, 2H, H_4), 8.61-8.69 (m, 4H, $H_{5,1}$), 8.05 (s, 2H, H_{10}), 7.81 (d, J = 9.2 Hz, 2H, H_8), 7.44-7.76 (m, 28H, $H_{Ph,2,3,6,7}$), 2.40-2.55 (m, 4H, P-CH_2-$(CH_2)_2$-CH_2-P), 1.80-1.94 (m, 4H_{CH2}, P-CH_2-(CH_2)$_2$-CH_2-P). ^{31}P{^{1}H} NMR (161.9 MHz $CDCl_3$, ppm): δ 37.2 (s). HR ESI-

MS (+) m/z: 1246.230 ([M+Na]$^+$, calc.: 1245.230). 1021.170 ([M-C≡Cphen]+, calc.: 1021.170). IR ($\bar{\upsilon}$, cm^{-1}): ν(C≡C) 2087 cm^{-1}; ν(C=C) 1486, 1450; ν(P-C) 1135.

Synthesis of **2a**

PPh_3 (13.1 mg, 0.05 mmol) was added to a solution of **2** (20 mg, 0.05 mmol) in 5 ml of CH_2Cl_2. The reaction mixture was stirred for 1 h at room temperature. The desired product was obtained after concentration of the solution under reduced pressure and precipitation with hexane (20 ml). The product was recrystallized with CH_2Cl_2/hexane yielding 14 mg (ɳ = 42%). ^{1}H NMR (400 MHz, CD_3Cl) δ 8.62 (d, J = 8.7 Hz, 1H, H_4), 8.57 (d, J = 8.6 Hz, 1H, H_5), 8.06 (d, J = 1.7 Hz, 1H, H_1), 7.85 (dd, J = 7.8, 1.5 Hz, 1H, H_3), 7.78 (dd, J = 8.6, 1.8 Hz, 1H, H_{10}), 7.72 – 7.64 (m, 4H, $H_{6\text{-}9}$), 7.63 – 7.53 (m, 7H, H_{Ph}), 7.53 – 7.44 (m, 8H, H_{Ph}). ^{31}P{^{1}H} NMR (162 MHz, CD_3Cl) δ-42.30 (s). HR ESI-MS(+) m/z: 683.119 ([M + Na]$^+$ calc.: 683.119). IR ($\bar{\upsilon}$, cm^{-1}): ν(C≡C) 2234; ν(C=C) 1487; 1430; ν(P-C) 1096.

Synthesis of **2b**

The synthesis of complex **2b** was performed following the same procedure of **2a** by modification of the PPh_3 by PMe_3 (4.4 µl of a commercial solution 1 M in THF, 0.05 mmol). Yield = 39% (9.2 mg). ^{1}H NMR (400 MHz, CD_3Cl) δ 8.64 (d, J = 8.2 Hz, 1H, H_4), 8.55 (d, J = 8.8 Hz, 1H, H_5), 8.04 (d, J = 2.2 Hz, 1H, H_1), 7.89 (d, J = 7.8 Hz, 1H, H_3), 7.79 – 7.71 (m, 2H, $H_{8,10}$), 7.65 (m, 3H, $H_{6,7,9}$), 1.33 – 1.22 (m, 9H, H_{Me}). ^{31}P{^{1}H} NMR (162 MHz, CD_3Cl) δ -10.34. HR HR ESI-MS(+) m/z: 512.503 ([M+K]$^+$, calc.: 512.504). IR ($\bar{\upsilon}$, cm^{-1}): ν(C≡C) 1991; ν(C=C) 1475, 1424; ν(P-C) 1085.

Synthesis of **2c**

The synthesis of complex **2c** was performed following the same procedure for **2a** but using $PNaph_3$ (20.6 mg, 0.05 mmol) instead of PPh_3. Yield = 41% (16.6 mg). ^{1}H NMR (400 MHz, CDCl3) δ 8.85 (d, J = 8.3 Hz, 3H), 8.58 (d, J = 8.2 Hz, 1H4), 8.49 (d, J = 8.7 Hz, 1H5), 8.05 (dd, J = 7.8, 1.8 Hz, 3H), 8.00 – 7.93 (m, 4+1H1), 7.82 (dd, J = 7.8, 1.5 Hz, 1H3), 7.69 – 7.63 (m, 2H10,8), 7.62 – 7.50 (m, 11H), 7.33 (m, J = 9.7, 6.1, 2.3 Hz, 3H9,6,7). ^{31}P{^{1}H} NMR (162 MHz, $CDCl_3$) δ 21.76. HR ESI-MS(+) m/z: 849.381 ([M+K]$^+$, calc.: 849.314). IR ($\bar{\upsilon}$, cm^{-1}): ν(C≡C) 2122 cm^{-1}; ν(C=C) 1451; 1429; ν(P-C) 1132.

Synthesis of **2d**

The synthesis of complex **2d** was performed following the same procedure of **2a** but using dppm (11.5mg, 0.03mmol) instead of PPh_3. Yield 11.7 mg (η = 50%). ^1H NMR (400 MHz, CD_3Cl) δ 8.56 (d, J = 7.7 Hz, $2H_4$), 8.50 (d, J = 8.6 Hz, $2H_5$), 7.98 (d, J = 1.8 Hz, $2H_1$), 7.79 (dd, J = 7.9, 1.5 Hz, $2H_3$), 7.71 (dd, J = 8.6, 1.8 Hz, $2H_{10}$), 7.66 – 7.59 (m, $10H_{Ph}$), 7.59 – 7.56 (m, $8H_{6-9}$), 7.45 – 7.38 (m, $10H_{Ph}$), 0.84 – 0.80 (m, $2H_{CH2}$). $^{31}P\{^1H\}$ NMR (162 MHz, CD_3Cl) δ-37.25. HR ESI-MS(+) m/z: 1203.190 ([M+Na^+], calc.: 1203.183); 979.125 ([M-C≡Cphen]), calc.: 979.120). IR ($\bar{\upsilon}$, cm^{-1}): ν(C≡C) 2094 cm^{-1}; ν(C=C) 1455, 1433; ν(P-C) 1102.

Synthesis of **2e**

The synthesis of complex **2e** was performed following the same procedure of **2a** but using dppb (25 mg, 0.059 mmol) instead of PPh_3. Yield 11.3 mg (η = 45%).

^1H NMR (400 MHz, CD_3Cl) δ 8.63 (d, J = 8.2 Hz, $2H_4$), 8.57 (d, J = 8.7 Hz, $2H_5$), 8.05 (d, J = 1.7 Hz, $2H_1$), 7.86 (dd, J = 7.8, 1.5 Hz, $2H_3$), 7.77 (dd, J = 8.6, 1.8 Hz, $2H_{10}$), 7.72 – 7.55 (m, $8H_{6-9}$), 7.43 (d, J = 7.8 Hz, $20H_{Ph}$), 2.41 (s-br, 4H P-CH_2-$(CH_2)_2$-CH_2-P), 1.75 (s-br, 4H P-CH_2-$(CH_2)_2$-CH_2-P). $^{31}P\{^1H\}$ NMR (162 MHz, CD_3Cl) δ 31.97. HR ESI-MS(+) m/z: 1245.100 ([M+Na^+], calc.: 1245.130); 1021.170 ([M-C≡Cphen]), calc.: 1021.170). IR ($\bar{\upsilon}$, cm^{-1}): ν(C≡C) 2105 cm^{-1}; ν(C=C) 1451, 1430; ν(P-C) 1104.

Acknowledgements

The authors are grateful to Samsung GRO Technologies for financial support, the Spanish Ministerio de Ciencia, Innovación y Universidades (AEI/FEDER, UE Project CTQ2016-76120-P and PID2019-104121GB-I00), and The Finnish Cultural Foundation Central Fund (grant number 00201148). FCT/MCTES is acknowledged for financial support through the Associate Laboratory for Green Chemistry, LAQV-REQUIMTE (UID/QUI/50006/2013) and through Project PTDC/QUI-QFI/32007/2017. We are indebted to Zeon Europe GmbH for providing us Zeonex 480.

References

[1] H. A. Collins, M. Khurana, E. H. Moriyama, A. Mariampillai, E. Dahlstedt, M. Balaz, M. K. Kuimova, M. Drobizhev, V. X. D. Yang, D. Phillips, A. Rebane, B. C. Wilson and H. L. Anderson, *Nat. Photonics*, **2008**, *2*, 420–424.

[2] S. Zhang, M. Hosaka, T. Yoshihara, K. Negishi, Y. Iida, S. Tobita and T. Takeuchi, *Cancer Res.*, **2010**, *70*, 4490–4498.

[3] G. Zhou, W.-Y. Wong, S.-Y. Poon, C. Ye and Z. Lin, *Adv. Funct. Mater.*, **2009**, *19*, 531–544.

[4] S. Baluschev, T. Miteva, V. Yakutkin, G. Nelles, A. Yasuda and G. Wegner, *Phys. Rev. Lett.*, **2006**, *97*, 143903.

[5] A. Mills, A. Lepre, B. R. C. Theobald, E. Slade and B. A. Murrer, *Anal. Chem.*, **1997**, *69*, 2842–2847.

[6] S. Reineke, F. Lindner, G. Schwartz, N. Seidler, K. Walzer, B. Lüssem and K. Leo, *Nature*, **2009**, *459*, 234–238.

[7] H. Shi, L. Song, H. Ma, C. Sun, K. Huang, A. Lv, W. Ye, H. Wang, S. Cai, W. Yao, Y. Zhang, R. Zheng, Z. An and W. Huang, *J. Phys. Chem. Lett.*, **2019**, *10*, 595–600.

[8] S. Hirata, *Adv. Opt. Mater.*, **2017**, *5*, 1700116.

[9] Kenry, C. Chen and B. Liu, *Nat. Commun.*, **2019**, *10*, 2111.

[10] S. Elumalai, J. R. Lombardi and M. Yoshimura, *Mater. Adv.*, **2020**, *1*, 146–152.

[11] A. Lázaro, C. Balcells, J. Quirante, J. Badia, L. Baldomà, J. S. Ward, K. Rissanen, M. Font-Bardia, L. Rodríguez, M. Crespo and M. Cascante, *Chem. - A Eur. J.*, **2020**, *26*, 1947–1952.

[12] A. Lázaro, C. Cunha, R. Bosque, J. Pina, J. S. Ward, K.-N. Truong, K. Rissanen, J. C. Lima, M. Crespo, J. S. Seixas de Melo and L. Rodríguez, *Inorg. Chem.*, **2020**, *59*, 8220–8230.

[13] Z. Zhao, H. Zhang, J. W. Y. Lam and B. Z. Tang, *Angew. Chemie Int. Ed.*, **2020**, *59*,

9888–9907.

[14] M. Osawa, M. Hoshino, M. Akita and T. Wada, *Inorg. Chem.*, **2005**, *44*, 1157–1159.

[15] L. Bischoff, C. Baudequin, C. Hoarau and E. P. Urriolabeitia, in *Advances in Organometallic Chemistry*, Elsevier Inc., 1st edn., **2018**, vol. *69*, pp. 73–134.

[16] A. Pinto, N. Svahn, J. C. Lima and L. Rodríguez, *Dalton Trans.*, **2017**, *46*, 11125–11139.

[17] (a) M. Pujadas and L. Rodríguez, *Coord. Chem. Rev.*, **2020**, *408*, 213179; (b) J. Cámara, O. Crespo, M. C. Gimeno, I. O. Koshevoy, A. Laguna, *Dalton Trans*., **2012**, *41*, 13891.

Isaura Ospino,a Ekaterina S. Smirnovac and Sergey P. Tunik

[18] A. J. Blake, H. Schmidbaur, N. Mirzadeh, S. H. Prive and S. K. Bhargava, *Inorg. Chem.* **2019**, *58*, 4954–4961.

[19] X.-Y. Wang, Y.-X. Hu, X.-F. Yang, J. Yin, Z. Chen and S. H. Liu, *Org. Lett.*, **2019**, *21*, 9945–9949.

[20] E. Aguiló, A. J. Moro, M. Outis, J. Pina, D. Sarmento, J. S. Seixas De Melo, L. Rodríguez and J. C. Lima, *Inorg. Chem.*, **2018**, *57*, 13423–13430.

[21] R. A. Vogt, T. G. Gray and C. E. Crespo-Hernández, *J. Am. Chem. Soc.*, **2012**, *134*, 14808–14817.

[22] J. Wei, B. Liang, R. Duan, Z. Cheng, C. Li, T. Zhou, Y. Yi and Y. Wang, *Angew. Chemie Int. Ed.*, **2016**, *55*, 15589–15593.

[23] L. Paul, S. Chakrabarti and K. Ruud, *J. Phys. Chem. Lett.*, **2017**, *8*, 1253–1258.

[24] E. Aguiló, A. J. Moro, R. Gavara, I. Alfonso, Y. Pérez, F. Zaccaria, C. F. Guerra, M. Malfois, C. Baucells, M. Ferrer, J. C. Lima and L. Rodríguez, *Inorg. Chem.*, **2018**, *57*, 1017–1028.

[25] R. Gao, X. Fang and D. Yan, *J. Mater. Chem. C*, **2019**, *7*, 3399–3412.

[26] A. J. Moro, J. Avó, M. Malfois, F. Zaccaria, C. Fonseca Guerra, F. J. Caparrós, L.

Rodríguez and J. C. Lima, *Dalton Trans.*, **2019**, *49*, 171–178.

[27] A. De Nisi, C. Bergamini, M. Leonzio, G. Sartor, R. Fato, M. Naldi, M. Monari, N. Calonghi and M. Bandini, *Dalton Trans.*, **2016**, *45*, 1546–1553.

[28] J. Arcau, V. Andermark, E. Aguiló, A. Gandioso, A. Moro, M. Cetina, J. C. Lima, K. Rissanen, I. Ott and L. Rodríguez, *Dalton Trans.*, **2014**, *43*, 4426–4436.

[29] A. Möller, P. Bleckenwegner, U. Monkowius and F. Mohr, *J. Organomet. Chem.*, **2016**, *813*, 1–6.

[30] F. J. Caparrós, M. Outis, Y. Jung, H. Choi, J. C. Lima and L. Rodríguez, *Molecules*, **2020**, *25*, 949.

[31] N. Svahn, A. J. Moro, C. Roma-Rodrigues, R. Puttreddy, K. Rissanen, P. V. Baptista, A. R. Fernandes, J. C. Lima and L. Rodríguez, *Chem. - A Eur. J.*, **2018**, *24*, 14654–14667.

[32] M. Weishäupl, C. Robl, W. Weigand, S. Kowalski and F. Mohr, *Inorganica Chim. Acta*, **2011**, *374*, 171–174.

[33] N. Svahn, I. Sanz, K. Rissanen and L. Rodríguez, *J. Organomet. Chem.*, **2019**, *897*, 170–177.

[34] J. Vicente, J. Gil-Rubio, N. Barquero, P. G. Jones and D. Bautista, *Organometallics*, **2008**, *27*, 646–659.

[35] L. Gao, D. V. Partyka, J. B. Updegraff, N. Deligonul and T. G. Gray, *Eur. J. Inorg. Chem.*, **2009**, 2711–2719.

[36] A. J. Moro, B. Rome, E. Aguiló, J. Arcau, R. Puttreddy, K. Rissanen, J. C. Lima and L. Rodríguez, *Org. Biomol. Chem.*, **2015**, *13*, 2026–2033.

[37] M. C. Blanco, J. Cámara, V. Fernández-Moreira, A. Laguna and M. C. Gimeno, *Eur. J. Inorg. Chem.*, **2018**, 2762–2767.

[38] A. Gutiérrez-Blanco, V. Fernández-Moreira, M. C. Gimeno, E. Peris and M. Poyatos, *Organometallics*, **2018**, *37*, 1795–1800.

[39] J. R. Shakirova, M. Shimada, D. A. Olisov, G. L. Starova, H. Nishihara and S. P. Tunik, *Zeitschrift für Anorg. und Allg. Chemie*, **2018**, *644*, 308–316.

[40] M. Ferrer, L. Giménez, A. Gutiérrez, J. C. Lima, M. Martínez, L. Rodríguez, A. Martín, R. Puttreddy and K. Rissanen, *Dalton Trans.*, **2017**, *46*, 13920–13934.

[41] A. A. Penney, G. L. Starova, E. V. Grachova, V. V. Sizov, M. A. Kinzhalov and S. P. Tunik, *Inorg. Chem.*, **2017**, *56*, 14771–14787.

[42] M. Iwasaki, Y. Shichibu and K. Konishi, *Angew. Chemie Int. Ed.*, **2019**, *58*, 2443–2447.

[43] N. C. Habermehl, M. C. Jennings, C. P. McArdle, F. Mohr and R. J. Puddephatt, *Organometallics*, **2005**, *24*, 5004–5014.

[44] P. De Frémont, N. M. Scott, E. D. Stevens and S. P. Nolan, *Organometallics*, **2005**, *24*, 2411–2418.

[45] J. Vicente, M. T. Chicote, M. M. Alvarez-Falcón and P. G. Jones, *Organometallics*, **2005**, *24*, 4666–4675.

[46] E. M. Barranco, O. Crespo, M. Concepción Gimeno, A. Laguna, P. G. Jones and B. Ahrens, *Inorg. Chem.*, **2000**, *39*, 680–687.

[47] P. Niermeier, L. Wickemeyer, B. Neumann, H.-G. Stammler, L. Goett-Zink, T. Kottke and N. W. Mitzel, *Dalton Trans.*, **2019**, *48*, 4109–4113.

[48] M. Osawa, M. Hoshino and D. Hashizume, *Chem. Phys. Lett.*, **2007**, *436*, 89–93.

[49] M. S. Alsaeedi, B. A. Babgi, M. A. Hussien, M. H. Abdellattif and M. G. Humphrey, *Molecules* **2020**, *25*, 1033.

[50] M. Mamiya, Y. Suwa, H. Okamoto and M. Yamaji, *Photochem. Photobiol. Sci.*, **2016**, *15*, 278–286.

[51] L. Rodríguez, M. Ferrer, R. Crehuet, J. Anglada and J. C. Lima, *Inorg. Chem.*, **2012**, *51*, 7636–7641.

[52] M. A. West, K. J. McCallum, R. J. Woods and S. J. Formosinho, *Trans. Faraday*

Soc., **1970**, *66*, 2135–2147.

[53] R.W.W. Hooft, *COLLECT* **1998**, Nonius BV, Delft, The Netherlands.

[54] Z. Otwinowski, W. Minor, *Methods in Enzymology, Macromolecular Crystallography, Part A* **1997**, 276, 307-326. Edited by C. W. Carter Jr & R. M. Sweet, New York: Academic Press.

[55] G. M. Sheldrick, *SADABS* Version 2008/2 **1996**, University of Göttingen, Germany.

[56] G. M. Sheldrick, *Acta Crystallogr. Sect. A Found. Adv.*, **2015**, *71*, 3–8.

[57] O. V. Dolomanov, L. J. Bourhis, R. J. Gildea, J. A. K. Howard and H. Puschmann, *J. Appl. Crystallogr.*, **2009**, *42*, 339–341.

[58] G. M. Sheldrick, *Acta Crystallogr. Sect. C, Struct. Chem.*, **2015**, *71*, 3–8.

[59] M. J. Frisch, G. W. T., H. B. Schlegel, G. E. Scuseria, M. A. Robb, J. R. Cheeseman, G. Scalmani, V. Barone, B. Mennucci, G. A. Petersson, H. Nakatsuji, M. Caricato, X. Li, H. P. Hratchian, A. F. Izmaylov, J. Bloino, G. Zheng, J. L. Sonnenberg, M. Hada, M. Ehara, K. Toyota, R. Fukuda, J. Hasegawa, M. Ishida, T. Nakajima, Y. Honda, O. Kitao, H. Nakai, T. Vreven, J. A. Montgomery, Jr., J. E. Peralta, F. Ogliaro, M. Bearpark, J. J. Heyd, E. Brothers, K. N. Kudin, V. N. Staroverov, T. Keith, R. Kobayashi, J. Normand, K. Raghavachari, A. Rendell, J. C. Burant, S. S. Iyengar, J. Tomasi, M. Cossi, N. Rega, J. M. Millam, M. Klene, J. E. Knox, J. B. Cross, V. Bakken, C. Adamo, J. Jaramillo, R. Gomperts, R. E. Stratmann, O. Yazyev, A. J. Austin, R. Cammi, C. Pomelli, J. W. Ochterski, R. L. Martin, K. Morokuma, V. G. Zakrzewski, G. A. Voth, P. Salvador, J. J. Dannenberg, S. Dapprich, A. D. Daniels, O. Farkas, J. B. Foresman, J. V. Ortiz, J. Cioslowski, D. J. Fox, Gaussian 09 (Revission B.1); Gaussian Inc.: Wallingford CT 2010., 1, mj frisch, gw trucks, hb schlegel, ge scuseria, ma robb, jr cheeseman, g. Scalmani, v. Barone, b. Mennucci, ga petersson et al., gaussian. *Inc., Wallingford CT* **2009**, *121*, 150-166.

[60] A. Becke, *J. Chem. Phys* **1993**, *98*, 5648.

[61] C. Lee, W. Yang, R.G. Parr, *Phys. Rev. B* **1988,** *37*, 785.

[62] F. Weigend, R. Ahlrichs, *Phys. Chem. Chem. Phys.* **2005,** *7*, 3297-3305.

[63] A. Schäfer, C. Huber, R. Ahlrichs, *J. Chem. Phys.* **1994**, *100*, 5829-5835.

[64] A. E. Reed, L. A. Curtiss, F. Weinhold, Chem. Rev. **1988**, *88*, 899-926.

[65] J. Tomasi, B. Mennucci, R. Cammi, *Chem. Rev.* **2005,** *105*, 2999-3094.

[66] M. E. Casida, C. Jamorski, K.C. Casida, D.R. Salahub, *J. Chem. Phys.* **1998**, *108*, 4439-4449.